J. N. Nilchi, R. Liu, S. Li, M. Akgul, T. O. Rocheleau, and C. T.-C. Nguyen, "Third-order intermodulation distortion in capacitive-gap transduced micromechanical filters," *Proceedings*, IEEE Int. Frequency Control Symp., Denver, Colorado, April 12-16, 2015, pp. 5-10, DOI: 10.1109/FCS.2015.7138782.

Third Order Intermodulation Distortion in Capacitive-Gap Transduced Micromechanical Filters

Jalal Naghsh Nilchi, Ruonan Liu, Scott Li, Mehmet Akgul, Tristan O. Rocheleau, and Clark T.-C. Nguyen
Berkeley Sensor and Actuator Center
University of California, Berkeley
Berkeley, California, USA
E-mail: jalal.naghsh.nilchi@berkeley.edu

***Abstract*— The third-order intermodulation distortion in properly terminated high-order bridged clamped-clamped beam (CC-beam) channel-select micromechanical filters has been measured for the first time and found to be appreciably higher than seen on unterminated stand-alone CC-beams. In particular, a three-resonator bridged 8-MHz filter with 140nm gaps posts a measured IIP_3 of 25dBm and 36dBm for two-tone offsets of 200kHz and 400kHz, respectively, which are much larger than the -11.7dBm for a stand-alone 9.2MHz CC-beam with 200kHz two-tone offset. For the case where the required minimum signal-to-noise ratio is 10dB, the IIP_3 of 36dBm translates to an impressive spurious-free dynamic range of 102.3dB. The result matches well the prediction of a new model for non-linearity that incorporates not only parallel-plate capacitor nonlinearity, but also the influence of the filter structure, where *Q*-loading by the termination reduces the degree of out-of-channel tone suppression, but also reduces the amplitude of resonator motion, which then improves the IIP_3. The full model incorporates these phenomena, plus dependencies on dc-bias, gap spacing, and electrode area.**

Keywords—Third-order intermodulation, micromechanical resonators, micromechanical filters, channel selection, capacitive-gap transducer.

I. Introduction

Channel-select filters like those of this work, capable of rejecting all interferer signals relax the dynamic range requirements on subsequent stages, e.g., the LNA and the mixer, thereby greatly reduce power consumption. However, the degree of interferer suppression depends strongly on the linearity of the filter, which if not sufficiently linear, can also generate intermodulation spurs even after rejecting interferers.

A recent 223-MHz capacitive-gap transduced disk micromechanical filter [1] proved that with electrode-to-resonator gaps on the order of 39nm, its transduction was sufficient to achieve a channel-select response with a small percent bandwidth of 0.09% and in-band insertion loss of 2.7dB, as well as a 50dB of out-of-channel rejection, all while maintaining a termination resistance around 500Ω which is easily *L*-network-matched to conventional antennas. However, use of such devices in RF communication circuits has so far been deferred due to skepticism on the linearity of these filters, which must satisfy the very strict specifications of present-day wireless standards. For example, the European GSM standard for mobile communications [2] requires a minimum total IIP_3 of -18dBm in the receiver path to insure adequate suppression of interferer signals from adjacent channels.

Previous works [3, 4, 5] on this issue were limited to two-tone measurements on single resonators, as opposed to multiple resonator filters. Pursuant to determining the linearity of high-order capacitive-gap micromechanical filters, this paper represents a complete analytical formulation for the IIP_3 of such devices and then verifies the formulation via experimental measurement on 3rd- and 4th-order 8-MHz clamped-clamped beam filters, shown in Fig. 1. With IIP_3 on the order of 36dBm for 400-

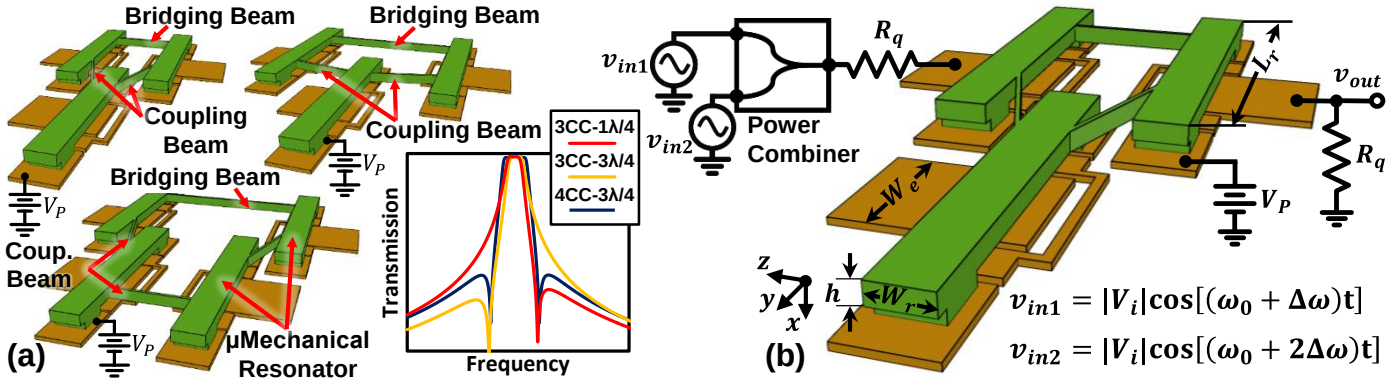

Fig. 1. (a) Perspective-view schematics for the three bridged micromechanical filter designs used in this work to measure nonlinearity in capacitive-gap filters and their frequency characteristics. (b) Two-tone experiment setup showing needed biasing, excitation, and sensing circuits along with CC beam dimensions. Tones are spaced equally from each other and from the center frequency of the filter.

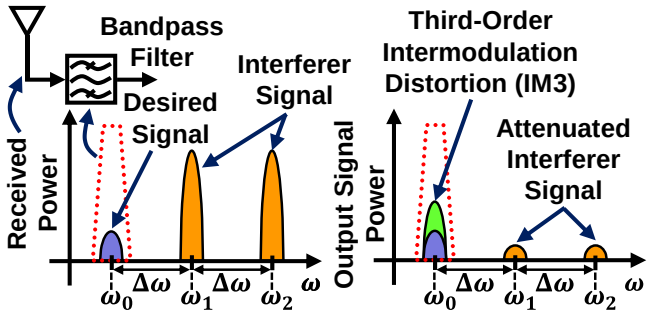

Fig. 2. While a channel-select filter attenuates out-of-band interferer signals, filter nonlinearity can still produce a troublesome intermodulation component at the output, especially if interferers are $\Delta\omega$ and $2\Delta\omega$ away from desired signal, for which the IM_3 component will be exactly at ω_0 and can deteriorate receiver signal-to-noise ratio, *SNR*.

kHz tone separations, these filters possess sufficient linearity for a large range of HF RF front-end or IF applications.

II. Analytical Model

Before presenting the model for multi-resonator filter nonlinearity, it is instructive to first review the existing formulation for stand-alone resonators. This section starts with intermodulation distortion fundamentals, then moves to deeper analysis of intermodulation distortion that accounts for more nonlinear terms than previous work [4], and culminates with a comprehensive formulation for multi-resonator filters.

A. Intermodulation Distortion Fundamentals

Any practical system that entails some nonlinearity is most conveniently modeled by a Taylor series:

$$y = a_0 + a_1 x + a_2 x^2 + a_3 x^3 + \cdots \tag{1}$$

where x and y are input and output and a_is describe system behavior. For the case of the third order intermodulation distortion, the input of consequence takes the form

$$x = S_0 \cos(\omega_0 t) + S_1 \cos(\omega_1 t) + S_2 \cos(\omega_2 t) \tag{2}$$

where two interferer signals at frequencies ω_1 and ω_2 add to the desired signal at frequency ω_0. When this signal passes through a nonlinear transfer function of the form in (1), the output includes not only a scaled version of the input, but also spurious signals at frequencies not present in the original input. Specifically, inserting (2) into (1), harmonics as well as intermodulation components arise

$$\begin{aligned} y = \cdots &+ a_1 S_0 \cos(\omega_0 t) + \frac{1}{2} a_2 S_0^2 \cos(2\omega_0 t) \\ &+ \frac{3}{4} a_3 S_1^2 S_2 \cos\big((2\omega_1 - \omega_2)t\big) + \cdots \end{aligned} \tag{3}$$

The harmonic terms occupy much higher frequencies, so can be filtered out easily. However, intermodulation between two equispaced input tones can produce output terms at frequencies near the desired signal. In particular, third-order nonlinearity can generate an output component exactly at the desired frequency if one tone is twice as far from ω_0 as the other one, as shown in Fig. 2 and Eq. (3). This third-order intermodulation component, IM_3, can directly impact the signal-to-noise ratio of the desired

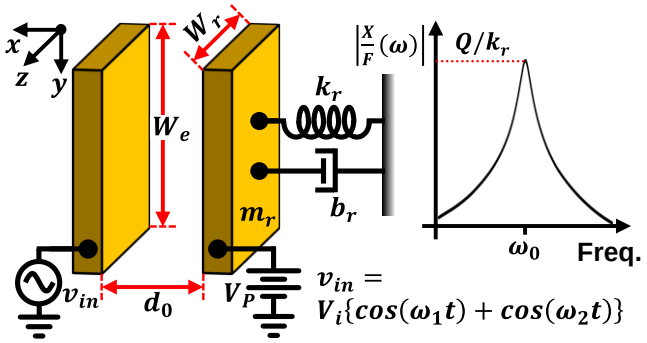

Fig. 3. Simplified schematic of a parallel-plate capacitive-gap transducer. The moving plate with effective stiffness and mass of k_r and m_r, respectively, produces the bandpass biquad frequency response shown on the right.

channel and eventually mask the channel completely, if the system nonlinearity is too large. Hence, IM_3 distortion must be constrained below a minimum acceptable value.

The third-order input intercept point (IIP_3) is defined as the input power level at which the extrapolated intermodulation component has the same power as the fundamental output. In general, a larger IIP_3 indicates smaller nonlinearity (or better linearity) in a given system and hence smaller intermodulation component generation, which is a design goal of communication systems.

As shown in Fig. 2, while a micromechanical channel-select filter attenuates out-of-channel interferer signals, its nonlinearity can still result in intermodulation components at its output that corrupt the desired signal, which motivates the necessity to design for maximum filter IIP_3. Note that interferer signals for a channel-select filter are outside the filter passband, unlike the case for a band-select filter, for which in-band interferers must be considered.

B. Capacitive-Gap Transducer Nonlinearity

Nonlinearity in either resonator stiffness [7] or capacitive-gap transduction [4] is often the most important contributors to filter nonlinearity. The former becomes significant when large displacement induces non-negligible internal strain in the resonator, which manifests as a stiffness nonlinearity. Since interferer signals are out-of-channel for a channel-select filter, the induced displacement is generally very small, so the stiffness nonlinearity is negligible. Therefore, transducer nonlinearity which translates to input force nonlinearity generates the intermodulation term of a channel-select filter.

As shown in Fig. 3, the transducers in the micromechanical filters of Fig. 1 are simplified to a parallel-plate capacitor composed of a gap spacing of d_0 separating two polysilicon electrodes: one fixed, the other suspended by an effective stiffness k_r. The transducer takes as input a dc voltage V_P applied to one electrode and an ac excitation voltage v_i applied to the other. Since no dc current flows through the capacitor, there is no dc power consumption. The free electrode moves in response to force F_{tot} generated by the input voltage combination following a biquad frequency response of Fig. 3, where the electrode effective stiffness k_r and quality factor Q determine the maximum displacement according to

$$\frac{X}{F}(\omega) = \frac{1}{k_r}\Theta(\omega) \tag{4}$$

$$\Theta(\omega) = \frac{1}{1-(\omega/\omega_0)^2 + j\omega/(Q\omega_0)} \tag{5}$$

where ω_0 is the resonance frequency from the ratio of k_r and effective mass m_r.

The actuation force F_{tot} that drives the resonator to move a displacement x derives from the co-energy in the capacitor [4]:

$$\begin{aligned} F_{tot} &= \frac{1}{2}\left(V_p - v_i\right)^2 \frac{\partial C}{\partial x} \\ &= \frac{1}{2}(V_P - v_i)^2 \frac{\partial}{\partial x}\left(C_0\left(1-\frac{x}{d_0}\right)^{-1}\right) \\ &= \frac{1}{2}(V_P - v_i)^2 \frac{C_0}{d_0}\left(1+\frac{2x}{d_0}+\frac{3x^2}{d_0^2}+\frac{4x^3}{d_0^3}+\cdots\right) \end{aligned} \tag{6}$$

where C_0 is the parallel-plate capacitance at rest, and d_0 is the electrode-to-resonator gap spacing, neglecting beam bending under applied dc-bias voltage V_P. For purposes of IIP_3 determination, the input voltage comprises the sum of two out-of-band signals:

$$v_i = V_1\cos(\omega_1 t) + V_2\cos(\omega_2 t) \tag{7}$$

The F_{tot} expression (6) has a second-order dependence on input voltage v_i, which combined with the nonlinear nature of the change in the capacitance per unit displacement $\partial C/\partial x$, results in higher order nonlinearities. In particular, out-of-band interferer signals at ω_1 and ω_2, equispaced from ω_0 and from each other ($\omega_1 - \omega_0 = \omega_2 - \omega_1$), induce small displacements at ω_1 and ω_2, respectively. Nonlinear interaction between these displacements and with the input voltages produces a displacement spur at ω_0 via third-order intermodulation terms, as shown in Fig. 4. Here, the total resulting resonator displacement takes the form:

$$\begin{aligned} x = X_0\cos(\omega_0 t + \phi_0) + X_1\cos(\omega_1 t + \phi_1) \\ + X_2\cos(\omega_2 t + \phi_2) \end{aligned} \tag{8}$$

where the ϕ_is are the relative phases between x and input voltage v_i, and the X_is are displacement amplitudes. The equation of motion governs the relation between F_{tot} and x:

$$m_r\ddot{x} + b_r\dot{x} + k_r x = F_{tot} \tag{9}$$

Neglecting nonlinear force terms, approximate expressions for the out-of-band X_1 and X_2 magnitudes take the form

$$X_1 = \frac{V_P V_1}{k_r}\frac{C_0}{d_0}\Theta(\omega_1) \tag{10}$$

$$X_2 = \frac{V_P V_2}{k_r}\frac{C_0}{d_0}\Theta(\omega_2) \tag{11}$$

If ω_1 and ω_2 are sufficiently distant from the center frequency ω_0, the approximate phases of the displacement components become

$$\phi_0 = 90°, \phi_1 = \phi_2 = 0 \text{ or } 180° \tag{12}$$

Substituting (10)-(12) into (8) and using this x in (6) yields the input force intermodulation term (13) shown at the bottom of the next page, where ε_0 is the permittivity in vacuum, $A_0 = W_r W_e$ is the electrode-to-resonator overlap area, $\Theta_1 = \Theta(\omega_1)$ and $\Theta_2 = \Theta(\omega_2)$.

The third-order input intercept point (IIP_3) is defined as the input power for which the third-order modulation IM_3 term is

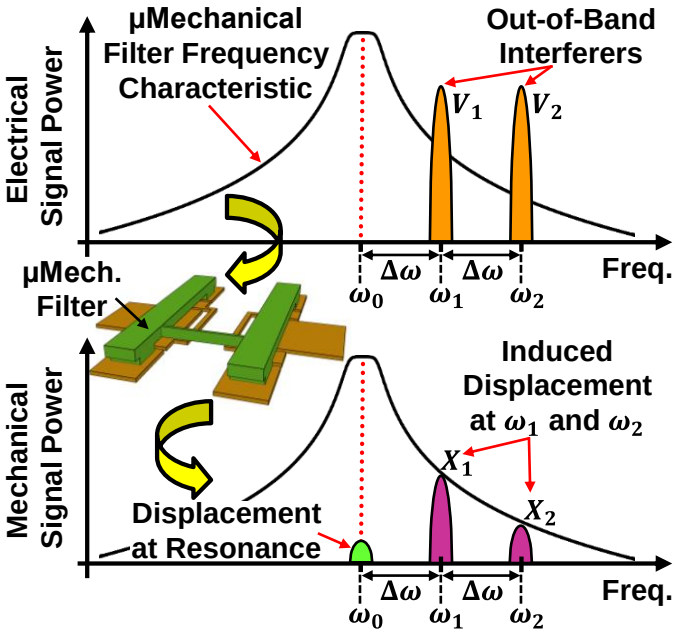

Fig. 4. Schematic description of IM_3 generation by two interferer signals going through a filter transfer function. The interaction between out-of-band motion induced by these interferers and input voltage can introduce an in-band input force and corresponding displacement. The undesirable IM_3 displacement results even with no input at resonance.

equal to the fundamental term. Assuming the nonlinearity associated with current generation at the output transducer is negligible compared to those associated with force generation at the input transducer, equating F_{IM3} (13) to the fundamental force F_{fund} (14) when exciting the resonator at ω_0, and then solving for V_i, yields the expression for input voltage V_{IIP3}, as given in (15). Recognizing that the linear force component is

$$F_{fund} = \frac{V_P \epsilon_0 A_0}{d_0^2} V_i \tag{14}$$

the corresponding input power, IIP_3, then takes the form

$$IIP_3 = \frac{V_{IIP3}^2}{2R_T} \tag{16}$$

where R_T is the total resistance in the system, seen at the input, dominated by the resonator motional resistance.

A careful examination of equation (15) shows that V_{IIP3} is dependent on not only material properties, but also resonator and electrode geometry. In particular, V_{IIP3} increases with decreases in V_P and A_0 and with increases in d_0 and k_r. Sine these parameters also affect the motional resistance R_x of micromechanical structure, there is a trade-off between the V_{IIP3} and the motional resistance of a capacitive-gap transducer.

C. Filter Considerations in IIP_3 Calculation

Although the parallel-plate approximation is still valid for a capacitive-gap micromechanical filter, the IIP_3 expression requires two major modifications to account for the following:

1) *Total Resistance*:

Proper termination is essential to minimize in-channel ripple and attain a flat passband. Before termination, the resonator Q's are too large and the filter passband consists of distinct peaks, as

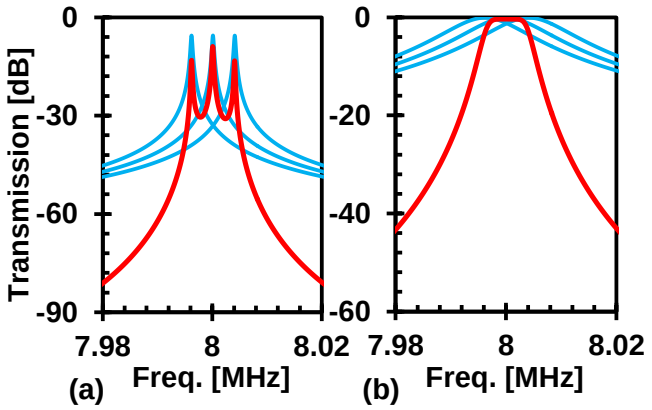

Fig. 5. Simulated frequency response spectra for an (a) unterminated and (b) terminated third-order filter alongside those for the three constituent resonators. Loading of resonator Q by termination reduces in-band displacement, but also reduces out-of-band attenuation. Still, the terminated filter provides more out-of-band rejection than a stand-alone resonator, which increases IIP_3.

shown in Fig. 5(a). The termination resistance needed to flatten the passband of a filter with center frequency f_0, bandwidth B, and small insertion loss is [8]:

$$R_q = \left(\frac{Q}{q_i Q_{fltr}} - 1\right) R_x \cong \frac{Q}{q_i Q_{fltr}} R_x \tag{17}$$

where $Q_{\text{fltr}}=f_0/B$. In contrast to the single resonator case, these termination resistors R_q dominate the resistance in the system, so $R_T \sim 2R_q$ in equation (16) when calculating the IIP_3 of filters.

2) *High-Order Mechanical System*:

The equation of motion (9) describes only single resonators, whereas the micromechanical filters of Fig. 1 comprise several resonators linked by coupling beams. Solving the complete mechanical system yields transfer functions listed in filter cook books, such as [8]. For example, the transfer function of a second-order filter coupled by quarter-wavelength coupling beams takes the form

$$\frac{X}{F}(\omega) = \frac{1}{k_r}\Theta(\omega) \tag{18}$$

$$\Theta(\omega) = \frac{1}{\left(1 - \frac{(\omega/\omega_0)^2}{1+P_{BW}} + \frac{j\omega}{Q_{fltr}\omega_0}\right)\left(1 - \frac{(\omega/\omega_0)^2}{1-P_{BW}} + \frac{j\omega}{Q_{fltr}\omega_0}\right)} \tag{19}$$

where P_{BW} is the filter percent bandwidth. Note that terminating the filter with R_q loads the quality factors of its end resonators, which is why Q_{fltr} appears in (19). The loading effect reduces resonator displacement at resonance ($X_0 \propto Q/k_r$) and reduces out-of-band rejection leading to larger out-of-band displacements X_1 and X_2. However, compared with a similarly terminated stand-alone resonator, the high-order transfer function of a multi-resonator filter shown in Fig. 5 provides a larger out-of-band attenuation that reduces out-of-band displacement, decreasing IM_3, hence increasing IIP_3.

III. Complete Formulation For IIP_3

While the parallel-plate capacitor approximation provides an analytical solution and design insight for the effect of third-order nonlinearities, it neglects phenomena such as beam bending due to dc-bias voltage and location-dependent effective stiffness. This can introduce errors in the IIP_3 calculation.

V_P-induced beam bending results in C_0 and d_0 of (10) and (11) that are not constant, but rather functions of location on the y-axis given by $d(y)$ in [5], neglecting variation along the z-axis. On the other hand, the effective resonator stiffness is also location dependent and changes according to the mode shape at the point of interest. For similar reasons, X_1 and X_2 vary along the beam length (the y-axis in Fig. 1(b)), approaching zero near the anchors. In general, with knowledge of the peak displacement (at the beam midpoint) governed by the resonator lumped model, displacements at other beam locations follow from the resonator mode shape. To correctly determine the total actuation force F_{tot}, intermodulation force components dF_{IM3} in infinitesimal regions dy at locations y should be integrated over the entire beam length.

Since effective stiffness increases dramatically moving away from the beam center, displacement is a strong function of location. This phenomenon can result in a V_{IIP3} value twice as large as that derived using a simple parallel-plate approximation. Including these modifications is essential to better explain the experimental results.

IV. Experimental Results

Third- and fourth-order clamped-clamped beam bridged micromechanical filters [9] like those of Fig. 1 were designed and fabricated to test the efficacy of the filter IIP_3 formulations. Besides the quarter-wavelength coupling beams connecting adjacent resonators to form the basic filter transfer functions, quarter- and third quarter-wavelength bridging beams also couple the first and last non-adjacent resonators [9] to provide parallel paths for mechanical signals from input to output. With proper

$$\begin{aligned} F_{IM3} = {} & V_i^5 \left\{ \frac{V_P^3}{k_r^3} \frac{(\epsilon_0 A_0)^4}{d_0^{11}} \left[\frac{9}{4}|\Theta_1|^2|\Theta_2| + \frac{9}{4}|\Theta_1||\Theta_2|^2 + |\Theta_1|^3 + \frac{3}{8}|\Theta_2|^3 \right] \right\} \\ & + V_i^3 \left\{ \frac{1}{4}\frac{V_P}{k_r} \frac{(\epsilon_0 A_0)^2}{d_0^5} \{2|\Theta_1| + |\Theta_2|\} \mp \frac{3}{4}\frac{V_P^3}{k_r^2} \frac{(\epsilon_0 A_0)^3}{d_0^8} \{|\Theta_1| + 2|\Theta_2|\}|\Theta_1| + \frac{3}{2}\frac{V_P^5}{k_r^3} \frac{(\epsilon_0 A_0)^4}{d_0^{11}} |\Theta_1|^2|\Theta_2| \right\} \end{aligned} \tag{13}$$

$$\begin{aligned} & V_{IIP3}^4 \left\{ \frac{V_P^2}{k_r^3} \frac{(\epsilon_0 A_0)^3}{d_0^9} \left[\frac{9}{4}|\Theta_1|^2|\Theta_2| + \frac{9}{4}|\Theta_1||\Theta_2|^2 + |\Theta_1|^3 + \frac{3}{8}|\Theta_2|^3 \right] \right\} \\ & + V_{IIP3}^2 \left\{ \frac{1}{4}\frac{1}{k_r} \frac{(\epsilon_0 A_0)}{d_0^3} \{2|\Theta_1| + |\Theta_2|\} \mp \frac{3}{4}\frac{V_P^2}{k_r^2} \frac{(\epsilon_0 A_0)^2}{d_0^6} \{|\Theta_1| + 2|\Theta_2|\}|\Theta_1| + \frac{3}{2}\frac{V_P^4}{k_r^3} \frac{(\epsilon_0 A_0)^3}{d_0^9} |\Theta_1|^2|\Theta_2| \right\} - 1 = 0 \end{aligned} \tag{15}$$

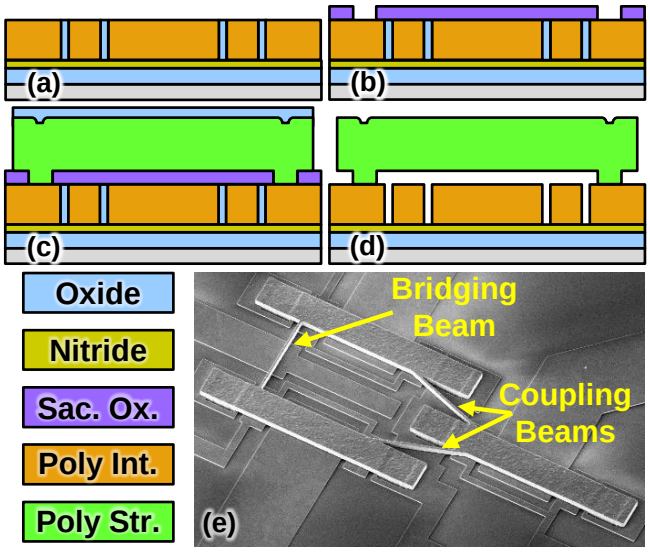

Fig. 6. (a)- (d) Cross-sections of the fabrication process flow used for the third- and forth-order bridged filter of this work. (e) SEM of a fabricated 3CC-λ/4 device.

design, these parallel paths are out of phase with the primary paths so insert a zero in the filter transfer function, effectively adding a notch in the filter frequency response and sharpening the passband-to-stopband roll-off. Each resonator in the filters of Fig. 1 has a tuning electrode to compensate any deviation in the resonator center frequency due to fabrication tolerances, which then enables near perfect (flat) passbands.

A. *Fabrication*

Filters were fabricated using a previously described vertical gap surface-micromachining process [5], summarized by the process cross-sections in Fig. 6, with some modifications to incorporate a damascene process to enable a thick, low resistance interconnect layer. Fabrication starts with deposition of 2μm-thick silicon dioxide and 400nm-thick silicon nitride on the silicon substrate to electrically isolate different interconnects. Then 1.5μm-thick of oxide is deposited and patterned using a negative interconnect mask to form a mold that defines thick interconnects after deposition of 2μm-thick polysilicon and polishing down to the oxide to yield Fig. 6(a). This damascene process removes all the structure topography, allowing for more precise definition of resonator center frequency. Next, 137nm of sacrificial oxide is deposited and patterned to open anchor vias, as shown in Fig. 6(b), followed by successive depositions of 2μm-thick structural P-doped-polysilicon and 500nm of oxide hard mask material, respectively. Patterning via the filter structure mask and etching then yields Fig. 6(c). A wet dip in hydrofluoric acid then releases devices, leaving free standing structures, such as shown in Fig. 6(d). Fig. 6(e) present the SEM of a released third-order λ/4-bridged micromechanical filter.

B. *Measurement Results*

Fig. 7 presents the frequency response spectra of the terminated bridged filters, biased at V_P and measured via the circuit shown in Fig. 1. These filters post in-band insertion losses and ripples on the order of ~1dB and 0.2dB, respectively, while also exhibiting respectable 40dB out-of-band rejections. Table 1 summarizes the filter characteristics.

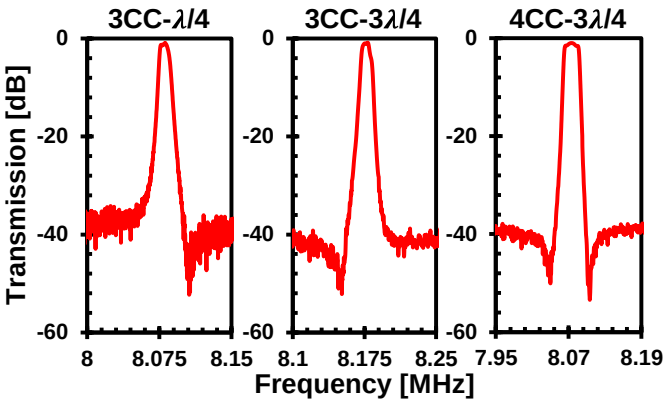

Fig. 7. Measured frequency responses of 3CC-λ/4, 3CC-3λ/4 and 4CC-3λ/4 terminated micromechanical filters like those of Fig. 1. The filters are biased at 21V, 20V and 22.5V and terminated by 12kΩ, 10kΩ and 20kΩ resistors, respectively. Tuning voltages were adjusted to yield flat passbands.

TABLE I. HF MICROMECHANICAL FILTER SUMMARY

Parameter	Designed/Measured		
	3CC-λ/4	3CC-3λ/4	4CC-3λ/4
μRes. Beam Length, L_r	40.8μm	40.8μm	40.8μm
μRes. Beam Width, W_r	8.0μm	8.0μm	8.0μm
μRes. Beam Thickness, h	2.0μm	2.0μm	2.0μm
Electrode Width, W_e	20.0μm	20.0μm	20.0μm
Gap Spacing, d_0	137nm	137nm	137nm
Coupling Beam Length, L_{s12}	22.3μm	22.3μm	22.3μm
Coupling Beam Length, $L_{s13\text{-}4}$	22.3μm	51.8μm	51.8μm
Coupling Beam Length, W_s	750nm	750nm	750nm
Coupling Location, l_{c12}	4.7μm	5.0μm	5.3μm
Coupling Location, $l_{c13\text{-}4}$	2.8μm	3.1μm	3.2μm
Filter Biasing Voltage, V_P	21V	20V	22.5V
Center Frequency, f_0	8.08MHz	8.18MHz	8.07MHz
Electromech. Coupling, C_x/C_0	14.77%	13.40%	16.96%
Resonator Quality Factor, Q	12,000	12,000	12,000
Bandwidth, B	10.7kHz	10.2kHz	26kHz
Percent Bandwidth, B/f_0	0.13%	0.12%	0.32%
Passband Ripple, PR	<0.2dB	<0.2dB	<0.2dB
Insertion Loss, IL	1.2dB	1.0dB	1.0dB
20dB Shape Factor	2.08	2.03	1.84
Stopband Rejection, SR	38dB	40dB	40dB
Predicted third-order input intercept point, IIP_3	(Δf = 400kHz) 36.2dBm	(Δf = 125kHz) 17.4dBm	(Δf = 80kHz) 23.0dBm
Measured third-order input intercept point, IIP_3	(Δf = 400kHz) 36.0dBm	(Δf = 125kHz) 17.0dBm	(Δf = 80kHz) 22.7dBm
Sp. Free Dyn. Range, $SFDR$ (SNR_{min} = 10dB)	(Δf = 400kHz) 102.3dB	(Δf = 125kHz) 89.94dB	(Δf = 400kHz) 91.0dB

Fig. 8 presents IIP_3 measurements on (a) a 3CC-3λ/4 bridged filter and (b) a 4CC-3λ/4 bridged filter. Here, a spectrum analyzer measured the output power response to two-tone inputs with frequency spacings like those pictured in Fig. 2. These filters show (a) an IIP_3 of 17dBm for a tone separation of 125kHz; and in (b), IIP_3's of 22.7dBm and 27dBm for tone separations of 80 and 160kHz, respectively.

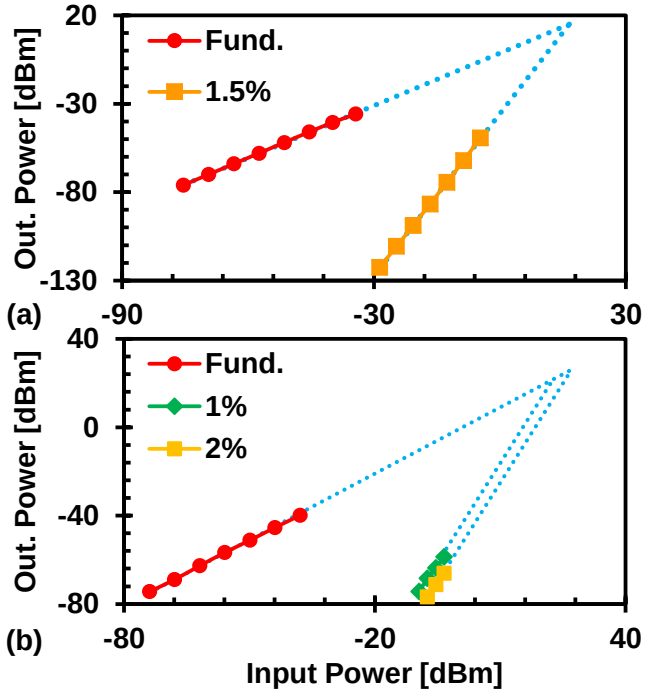

Fig. 8. Third-order input intercept point IIP_3 measurements of the (a) 3CC-3λ/4 and (b) 4CC-3λ/4 bridged micromechanical filters.

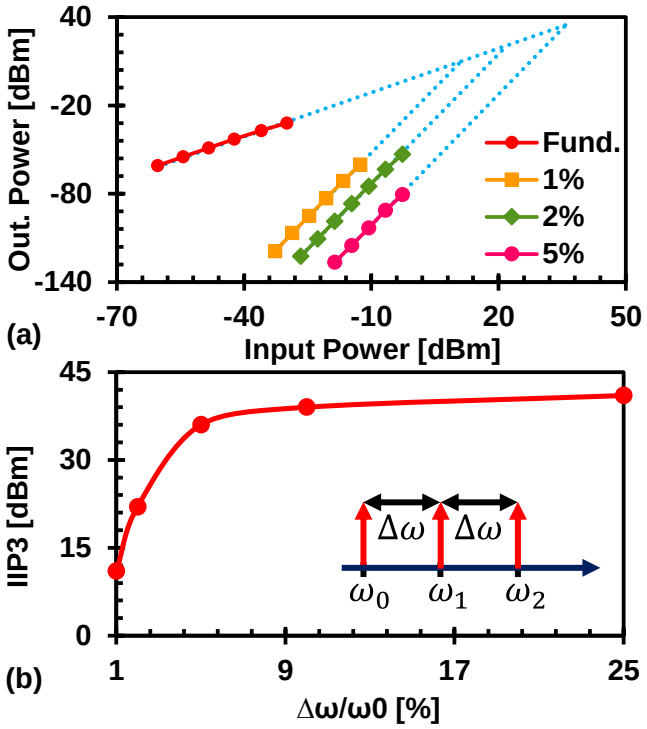

Fig. 9. (a) Two-tone measurement with tone separations of 80, 160 and 400kHz and (b) measured IIP_3 versus percent tone separation ($\Delta\omega/\omega_0$) for a terminated 3CC-λ/4 filter.

The expression for out-of-band spurious-free dynamic range takes the form [10]:

$$SFDR = \frac{2}{3}(IIP_3 + 174dBm - IL - 10\log(B)) - SNR_{min} \quad (20)$$

where SNR_{min} is the required minimum signal-to-noise ratio. Assuming SNR_{min}=10dB, these IIP_3's correspond to $SFDR$'s of 89.94dB for the 3CC-3λ/4 bridged filter with 125kHz tone separation; and 91dB and 93.9dB for the 4CC-3λ/4 bridged filter with 80 and 160kHz tone separations, respectively.

Fig. 9 presents IIP_3 measurements on a 3CC-λ/4 bridged micromechanical filter. Specifically, (a) shows two-tone measurements for different tone spacings, while (b) plots measured IIP_3 as a function of percent tone spacing ($\Delta\omega/\omega_0$). As expected, as out-of-band interferers move further away from the center frequency, induced displacements X_1 and X_2 decrease and IIP_3 increases. This filter achieves IIP_3 of 11dBm, 22dBm and 36dBm corresponding to $SFDR$'s of 85.67dB, 93dB and 102.34dB for tone separations of 80, 160 and 400kHz, respectively. These IIP_3's are more than 30dBm higher than previous marks for single resonators [4, 5].

V. Conclusion

The analytical expression for multi-resonator capacitive-gap transduced channel-select CC-beam bridged micromechanical filters not only matches measured IIP_3's as high as 36dBm for a tone separation of 400kHz, but also provides insight into just how good the linearity of such filters can be. In particular, the formulation shows that capacitive-gap transducer nonlinearity depends on not only material properties, but also on structure and electrode geometry, all of which serve as knobs through which one might design for a specific linearity requirement. Channel-select filters like those of this work, capable of rejecting all interferer signals and passing only the desired signal, and doing so with the high IIP_3's demonstrated, stand to greatly reduce dynamic range requirements on subsequent stages, in turn enabling much longer battery lifetimes for ultra-low power wireless front-ends.

Acknowledgment

The work was supported by DARPA.

References

[1] M. Akgul *et al*, "A passband-corrected high rejection channel-select micromechanical disk filter," *IFCS*, 2014.

[2] J. C. Rudell *et al*, *An Integrated GSM/DECT Receiver: Design Specifications*, UCB Electronics Research Laboratory Memorandum.

[3] Y.-W. Lin *et al*, "Third-order intermodulation distortion in capacitively-driven VHF micromechanical …," *IUS*, 2005.

[4] R. Navid *et al*, "Third-order intermodulation distortion in capacitively-driven CC-beam …," *MEMS*, 2001.

[5] F. Bannon *et al*, "High-Q HF micromechanical filters," *JSSC*, vol. 35, no. 4, pp. 512-526, 2000.

[6] W. Sahyoun *et al*, "Acoustic, piezoelectric, and dielectric nonlinearities of AlN in coupled resonator filters… ," *Trans. on UFFC*, vol. 58, no. 10, pp. 2162-2170.

[7] A. Shooshtari *et al*, "Nonlinear forced vibration analysis of clamped functionally graded beams ," *Acta Mechanica*, vol. 221, no. 1-2, pp. 23-38, 2011.

[8] A. I. Zverev, Handbook of Filter Synthesis, New Yok: John Wiley & Sons, 1967.

[9] S.-S. Li et al, "Bridged micromechanical filters," in *IFCS*, 2004.

[10] B. Razavi, RF Microelectronics, Prentice-Hall, 2011.